J. Am. Soc. Mass Spectrom. (2017)
DOI: 10.1007/s13361-017-1783-z

RESEARCH ARTICLE

Oligo p-Phenylenevinylene Derivatives as Electron Transfer Matrices for UV-MALDI

Laura J. Castellanos-García,[1] Brian Castro Agudelo,[2] Hernando F. Rosales,[1] Melissa Cely,[2] Christian Ochoa-Puentes,[2] Cristian Blanco-Tirado,[1] Cesar A. Sierra,[2] Marianny Y. Combariza[1]

[1]Escuela de Química, Universidad Industrial de Santander, Bucaramanga, Santander, Colombia
[2]Departamento de Química, Universidad Nacional de Colombia, Bogotá, Colombia

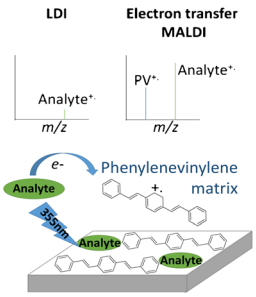

Abstract. Phenylenevinylene oligomers (PVs) have outstanding photophysical characteristics for applications in the growing field of organic electronics. Yet, PVs are also versatile molecules, the optical and physicochemical properties of which can be tuned by manipulation of their structure. We report the synthesis, photophysical, and MS characterization of eight PV derivatives with potential value as electron transfer (ET) matrices for UV-MALDI. UV-vis analysis show the presence of strong characteristic absorption bands in the UV region and molar absorptivities at 355 nm similar or higher than those of traditional proton (CHCA) and ET (DCTB) MALDI matrices. Most of the PVs exhibit non-radiative quantum yields (ϕ) above 0.5, indicating favorable thermal decay. Ionization potential values (IP) for PVs, calculated by the Electron Propagator Theory (EPT), range from 6.88 to 7.96 eV, making these oligomers good candidates as matrices for ET ionization. LDI analysis of PVs shows only the presence of radical cations ($M^{+\cdot}$) in positive ion mode and absence of clusters, adducts, or protonated species; in addition, $M^{+\cdot}$ threshold energies for PVs are lower than for DCTB. We also tested the performance of four selected PVs as ET MALDI matrices for analytes ranging from porphyrins and phthalocyanines to polyaromatic compounds. Two of the four PVs show S/N enhancement of 1961% to 304% in comparison to LDI, and laser energy thresholds from 0.17 μJ to 0.47 μJ compared to 0.58 μJ for DCTB. The use of PV matrices also results in lower LODs (low fmol range) whereas LDI LODs range from pmol to nmol.

Keywords: Electron transfer, UV-MALDI, p-Phenylenevinylene matrix, Optoelectronic, Ionization potential, Quantum yield, Porphyrins, Polyaromatics, Phthalocyanine

Received: 1 April 2017/Revised: 10 August 2017/Accepted: 10 August 2017

Introduction

Gas-phase protonation, deprotonation, and adduct formation reactions are very common to MALDI-MS; however, not all organic compounds are amenable to charge acquisition through these processes. The electron transfer (ET) process, a less travelled road in MALDI-MS, can expand the usefulness of the technique because it allows ionization of compounds essential to material sciences such as polymers, fullerenes, polycyclic aromatic hydrocarbons, organometallic, and coordination complexes [1–6]. In positive mode ET ionization, primary ions of the matrix (radical cations) react with neutral analyte molecules in the gas phase. The electron transfer process, from the neutral to the ionized matrix, occurs only if the ionization potential of the matrix is higher than the ionization potential of the analyte ($IP_M > IP_A$) as first reported by McCarley [7].

Highly conjugated phenylenevinylene (PV) systems are amongst the most studied architectures in organic polymers for photophysical applications [8–10]. It is well known that photoluminescence and electroluminescence phenomena in PVs depend of many physicochemical factors, amongst which molar absorption coefficients and maximum absorption wavelengths in the UV-VIS region play a major role [10, 11]. Although currently there are no reports of PVs as MALDI matrices, basic research related to their solid-state behavior and photophysical properties indicates potential usefulness

Electronic supplementary material The online version of this article (https://doi.org/10.1007/s13361-017-1783-z) contains supplementary material, which is available to authorized users.

Correspondence to: Marianny Combariza; *e-mail:* marianny@uis.edu.co

Published online: 06 September 2017

for this particular application. The structural versatility of PVs, easily accessed by manipulation of the electronic conjugation length or the chemical nature of the substituents in these molecules [12–15], allows not only fine control of photophysical behavior (e.g., absorption/emission wavelengths and quantum efficiencies), but also of solubility and stability properties, which are key factors in MALDI matrices. A series of studies report interesting solid crystal properties for PVs such as the enhancement in photophysical properties by aggregation of PVs through π stacking by Amrutha and Jayakannan [16], and the capability of PVs to undergo photo-induced intra- and intermolecular energy and charge transfer processes like those occurring in primary and secondary reactions in the MALDI plume [17–20]. In addition, Samori et al. showed that electronic conjugated systems such as stilbenes, basic units of PVs, are able to produce radical cations during irradiation with a 355 nm Nd:YAG laser [21]. Finally, Grozema et al. using theoretical approximations described the formation of positively charged species (radical cations) from PVs with the ability to maintain high absorption coefficients with minor changes in molecular geometry [22].

The combination of a wide array of molecular properties makes an efficient ET matrix, among others relatively high IPs, high molar absorptivity in the solid state, good solubility properties, appropriate crystallization, vacuum stability, and low tendency to form clusters. Many structures for ET purposes have been tested, mostly through trial and error; however currently ET matrices are mostly based on highly conjugated aromatic compounds such as DCTB and 9-nitroanthracene. As examples, Chait et al. successfully obtained radical cations of phthalocyanines, porphyrins, and multiporphyrin arrays using 1,4-benzoquinone [23], whereas Boltalina et al. studied the ionization of synthetic fluorofullerenes in negative mode using 9-nitroanthracene, the latter, also hindered defluorination of the substituted fullerenes, a reaction observed when using LDI [3, 24]. However, Drewello et al., performing the same experiment on positive ion mode, found two major problems with the use of 9-nitroanthracene. The first related to an oxygen transfer reaction from the matrix to the analyte, and the second associated with the presence of abundant clusters in the low mass region of the spectrum (from *m/z* 220 to 800) interfering with the analysis of low molecular weight analytes [5].

In 2000, Luftmann et al. [25] introduced the most successful to-date electron transfer matrix, commonly known as DCTB (*trans*-2-[3-(4-tert-butylphenyl)-2-methyl-2-propenylidene] malononitrile). DCTB is useful for the ionization of fullerenes derivatives [3, 25], polymers [25, 26], and porphyrins [27], among others [28]. The advantages of DCTB, over other ET matrices, lie in the relatively low laser fluence needed for ionization and its ability to prevent fragmentation of labile analytes [5, 23, 25]. However, there are still some issues regarding the performance of DCTB such as formation of adduct ions with analytes containing amine-groups. The carbon adjacent to the dicyanomethylene functionality in DCTB can act as an electrophile for primary and secondary aliphatic amines, leading to the formation of imines [29]. More recently, 9,10-diphenylanthracene (9,10-DPA) was reported as MALDI matrix for the ET ionization of model analytes like chlorophyll and retinol [30]; this compound and its derivatives are commonly used in OLEDS [31] and as reactants in electron transfer dissociation ETD [32]. However, the photophysical characteristics of 9,10-DPA, e.g., IP (7.0 eV) and ε_{355nm} (7220 L mol^{-1} cm^{-1}) [30], are not superior to established ET matrices like DCTB, IP (8.5 eV) [33] and ε_{355nm} (33980 L mol^{-1} cm^{-1}) [25].

In an interesting review Wyatt [1] highlights the usefulness of MALDI for the analysis of coordination and organometallic complexes and points out the lack of research in this area despite the great benefits of the technique. For instance, porphyrins and phthalocyanines are ionized through radical cation formation and LDI is the technique of choice for their analysis; however, LDI induces demetallation and increases fragmentation in labile analytes [5, 23]. Other analytes such as polycyclic aromatic hydrocarbons (PAH), with low solubility in polar solvents, are also susceptible to electron transfer ionization. Solvent-free LDI analysis was put forward as an alternative for the ionization of these non-polar analytes; however, molecular cation abundances and survival yields in this technique are very low [34].

Considering the wide applicability of ET ionization for the analysis of polymers, fullerenes, polycyclic aromatic hydrocarbons, organometallic, and coordination complexes [1], in this contribution we report the synthesis, photophysical, and mass spectrometric characterization of eight PV derivatives with potential application as ET MALDI matrices. We also test the performance of four of these structures (PV-CN, PV-COOH-CH_3, PV-COOH-OCH_3, and PV-Cl) as electron transfer MALDI matrices for the analysis of labile compounds such as phthalocyanines, porphyrins, and polycyclic aromatic hydrocarbons (PAH). In this regard, we compare the effectiveness of the PV derivatives as ET MALDI matrices, in terms of molecular ions energy threshold, S/N, and limit of detection (LOD), with traditional LDI analysis and MALDI using DCTB as ET standard matrix.

Experimental

Chemicals

Unless otherwise stated, all compounds are commercially available and were used without further purification. DMSO, DMF, $CHCl_3$, THF, acetonitrile, p-xylene, methanol, n-hexane, ethyl acetate, terephthalaldehyde, dimethoxybenzene, potassium tert-butoxyde, and methanol were purchased form Merck (Darmstadt, Germany). Methyl triphenylphosphonium bromide, methyl 4-Iodo benzoate, and sodium periodate were purchased from Panreac (Barcelona, Spain). $Pd(dba)_2$, triphenyl phosphite, boron tribromide, 2-chloroethanol, 4-vinyl benzoic acid, anthracene, 5,10,15,20-tetrakis(4-methoxyphenyl)-21H,23H-porphine cobalt (II) (cobalt porphyrin), zinc 29H,31H-phthalocyanine (zinc phthalocyanine), coronene, 2,3-naphthalocyanine (naphthalocyanine), rubrene, 29H,31H-phthalocyanine (phthalocyanine), MALDI grade α-CHCA, and MALDI grade trans-2-

[3-(4-tert-butylphenyl)-2-methyl-2-propenylidene (DCTB) were purchased form Sigma-Aldrich (St. Louis MO, USA).

PVs Derivatives synthesis

Scheme 1 depicts the general procedure for PV synthesis and the structure of the eight molecules tested as MALDI matrices. PV synthesis starts by preparation of a series of styrene and iodobenzene precursors, followed by coupling reactions. The iodobenzene precursors are obtained through a S_EAr mechanism by refluxing appropriate reactants with KIO_3 and I_2 in acid media [19]. On the other hand, following the Wittig olefination the corresponding aromatic aldehydes are subsequently converted (in high yield) to their styrene derivatives using methyl triphenyl phosphonium bromide and the appropriate base [15]. Finally, the iodobenzene and styrene derivatives are connected by means of the Mizoroki-Heck coupling reaction using $Pd(dba)_2$ and triphenylphosphite, according to our previously reported methodology [35]. In the case of compounds with carboxylic functional groups, an extra hydrolysis step was needed after the final coupling reaction. Full synthetic details and spectroscopic characterization of all precursors and target compounds are provided in section S1 of the Supplemental information.

UV-vis Spectroscopy Measurements

UV-vis spectra for the PVs derivatives and the standard matrices were acquired at 22 °C using 12.5 μM solutions of the compounds in DMSO and a double channel Shimadzu UV-2401PC spectrophotometer (Kyoto, Japan) with a scanning range of 200 to 700 nm. Molar absorptivity (ε) at λ_{355nm} was calculated using the Beer-Lambert law for serial dilutions, from 2 to 25 μM, of PV derivatives in DMSO correlation coefficients for the measurements are higher than 0.97 (See section S2 of the Supplemental Information).

Quantum Yield Measurements

Quantum yields were measured with a PTI/QM 40 Spectrofluorometer (NJ, USA) with an excitation wavelength of 355 nm and fluorescence emission monitoring in the range of 360 to 700 nm. Anthracene and quinine sulphate were used as reference fluorophores for intercrossing calibration. PV derivatives, anthracene and quinine sulphate concentrations in solution were adjusted to yield a UV-vis absorbance of approximately 0.05 for all fluorescence experiments; this translates in solutions ranging from 2 to 20 μM in DMF. Calibration curves were prepared in ethanol for anthracene and in a 0.1 M solution of H_2SO_4 in deionized water for quinine sulphate [36, 37]. The calculated error for the intercrossing calibration was less than 5%.

Theoretical Calculations

PVs and analytes vertical ionization potentials (IPs) were determined by the Electron Propagator Theory (EPT) using the Gaussian 09 software suite [38]. Closed shell HF/6-311G(d,p)-optimized geometries were used to start EPT calculations using the same basis set [39, 40]. EPT simulations of all PVs exhibited pole strengths above 0.85 giving credence to their ability to reproduce the experimental data.

LDI and UV-MALDI Sample Preparation

For PVs LDI analysis, 2.5 mM stock solutions of the PVs derivatives in THF were prepared. Because of the low solubility of some of the PVs, specifically PV-COOH and PV-$COOH-CH_3$, stock solutions were placed on a Bransonic ultrasonic bath (Danbury CT, USA) at 40 KHz and 130 W during times ranging from 1 to 20 min, depending on the PV solubility; 1.0 μL of each solution was placed on a stainless steel target and let dry at room temperature. For MALDI analysis, 2.5 mM stock solutions of the PV derivatives (PV-CN, PV-$COOH-CH_3$, PV-$COOH-OCH_3$, and PV-Cl) in THF were prepared. For all analytes, 2.5 mM stock solutions were prepared and diluted to 25, 5, and 2.5 μM. Equal volumes of the PVs and analyte solutions were mixed (1500 rpm for 15 min) to reach analyte-to-matrix molar ratios of 1:100, 1:500, and 1:1000; 1 μL of each mixture was applied to the sample target using the dried droplet method.

Mass Spectrometry

A Bruker Ultraflextreme MALDI TOF-TOF instrument (Bruker Daltonics, Billerica, MA, USA) was used to perform MALDI and LDI analyses. The instrument is equipped with a 1 kHz Smart Beam Nd:YAG laser (355 nm), with a maximum

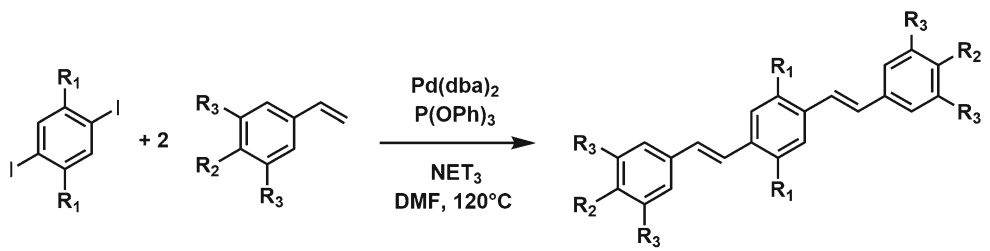

PV-COOH	R_1: H, R_2: COOH, R_3: H	**PV-Cl**	R_1: OCH_3, R_2: Cl, R_3: H
PV-$COOH-CH_3$	R_1: CH_3, R_2: COOH, R_3: H	**PV-NO_2**	R_1: OCH_3, R_2: NO_2, R_3: H
PV-$COOH-OCH_3$	R_1: OCH_3, R_2: COOH, R_3: H	**PV-OH**	R_1: OCH_2CH_2OH,R_2: OCH_3, R_3: OCH_3
PV-CN	R_1: H, R_2: CN, R_3: H	**PV-OCH_3**	R_1: OCH_3, R_2: OCH_3, R_3: OCH_3

Scheme 1. General procedure for PV synthesis using the Mizoroki-Heck cross coupling reaction

energy output of approximately 8.5 μJ per shot; 6 ns pulse and average spot size of 100 μm, according to the manufacturer's specifications. For matrices threshold energies laser power was varied from 0.14 to 2.5 μJ per pulse using the instrument's attenuator. The energy output of the laser was measured using a PowerMax-USB UV/vis Wand (Coherent, Santa Clara, CA, USA); all laser power measurements were performed by triplicate. Positive ion mass spectra, from *m/z* 180 to 2000, were acquired in reflectron mode with delayed extraction set at 100 ns, and an accelerating voltage of 25 kV. Instrument calibration was performed using CHCA and a mixture of standard peptides: leu-enkephaline, bradykinin, bombesin, and renin substrate purchased from Sigma Aldrich (St. Louis, MO, USA).

To ensure unbiased data acquisition, we used an autoexecution method within the FlexControl software (Bruker Daltonics, Billerica, MA, USA) of the instrument. The autoexecution method uses a random walk algorithm, which takes 10 laser shots in the same coordinates, then the target moves to another random position until it completes the requested total shots, in this case 500. If the summed spectra fit the evaluation parameters, they are added to the total spectrum, if they do not then another acquisition takes place; each reported analysis corresponds to the sum of 2000 spectra. Data analysis was performed using the FlexAnalysis software (Bruker Daltonics, Billerica, MA, USA). The software automatically reports ion abundances, S/N ratios, signal resolution, peak area, and monoisotopic masses. Experimental and theoretical isotope patterns, calculated with ChemCalc [41], were compared to verify compound identification.

Results and Discussion

UV-vis Characterization

Many reports regarding photophysical properties of oligo PVs, particularly optical absorption and photoluminescence, are available in literature [12, 19, 42–44]. There is general agreement that substituent types and their placement in the PV core strongly influence PV derivatives optical performance [12, 13, 42, 43]. Typically, the presence of alkyl or alkoxy groups on the central ring improves compound solubility [12, 45]; while substituents in the peripheral rings induce shifts in UV-vis absorption and fluorescence emission wavelengths. By using PV (1,4-distyrylbenzene) as core structure, we introduced weak and medium electron-donating groups (-CH_3, -OCH_3, and –OC_2H_4OH) on the central phenylene ring (Position R_1, Scheme 1), and both electron-donating (-OCH_3) and electron-withdrawing groups (-CN, -Cl, -NO_2, -COOH) on the peripheral rings (Positions R_2 and R_3, Scheme 1). For some of the selected structures (PV-CN, PV-COOH, PV-Cl, PV-NO_2, PV-OH and PV-OCH_3) basic photophysical, spectroscopic and physicochemical characteristics were available from previous works; [18, 19, 46–48] while the molecules PV-COOH-CH_3 and PV-COOH-OCH_3 have not been previously reported.

Figure 1 shows UV-vis absorption spectra for the tested PV series, molar absorptivities (ε) at λ_{355nm}, solubility data and maximum absorption wavelengths (calculated by derivation of the spectral functions). In accordance with previous reports [12, 43], PV derivatives exhibit two characteristic strong absorption bands ranging from 300 to 390 nm and 320 to 520 nm. As expected the presence and position of various functional groups on the phenylenevinylene core causes displacements in the experimental absorption wavelengths, starting from the blue shifted absorption bands in PV-COOH-CH_3 (at 367 nm) and ending with the red shifted bands of PV-NO_2 (at 447 nm). We calculated the effective wavelength shift (fourth column in Figure 1) for each compound as the difference between the experimental maximum absorption wavelengths for the PV derivative and the maximum absorption wavelength reported in literature for the PV core (381 nm). Previously, Heller *et al.* [43] published the physicochemical and photophysical characterization of the PV core; however due to poor solubility this compound was never used in electroluminescence applications. We can establish a trend when examining PV derivatives UV-vis spectra: clearly the presence of electron withdrawing groups, -NO_2 and –Cl, in the terminal phenylenes (R_2 positions, Scheme 1) produces a bathochromic (red) shift of 66 and 18 nm respectively with respect to the maximum absorption wavelength of the PV core (381 nm). This shift is due probably to an increase in effective π conjugation length in the excited state, as has been previously reported [42, 43]. The presence of alkoxy groups, with moderate electron donating capabilities, still induces a red shift on the maximum absorption band corresponding to 27, 17 and 14 nm for the PV-COOH-OCH_3, PV-OCH_3 and PV-OH structures, respectively. On the other hand, the presence of –COOH and -CN groups in the side rings causes a hypsochromic (blue) shift in absorption maxima of 6, 14 and 9 nm for PV-COOH, PV-COOH-CH_3 and PV-CN, respectively. Blue shifts are attributed to substituents that prevent planarization by reducing effective π conjugation length in the excited state as has been previously reported [42, 43].

MALDI-relevant UV-vis absorption bands located between 300 and 400 nm, corresponding to π-π* transitions of the phenyl and vinyl groups, are common to all of the tested PV derivatives. According to Figure 1 all absorption maxima for PV derivatives lie to the right of the 355 nm value. PV-COOH, PV-CN and PV-COOH-CH_3 exhibit the closest absorption wavelengths to the 355 nm line, with λ_{max} of 367, 372 and 375 nm respectively; these molecules have a slight red shift of 12, 17 and 20 nm with respect to the laser wavelength. Although PV-Cl, PV-OH, PV-OCH_3 and PV-COOH-OCH_3 are further red-shifted than both acid and cyano PV derivatives, they still exhibit significant absorption at 355 nm. Finally, PV-NO_2 has the most dramatic shift to red wavelengths: 92 nm from the 355 nm value, due to effect of the electron withdrawing functional group.

Commercial MALDI instruments operate at fixed wavelength values of 337 and 355 nm for N_2 and Nd:YAG lasers, respectively; thus, UV-MALDI experiments in these instruments necessarily require a matrix that efficiently produces

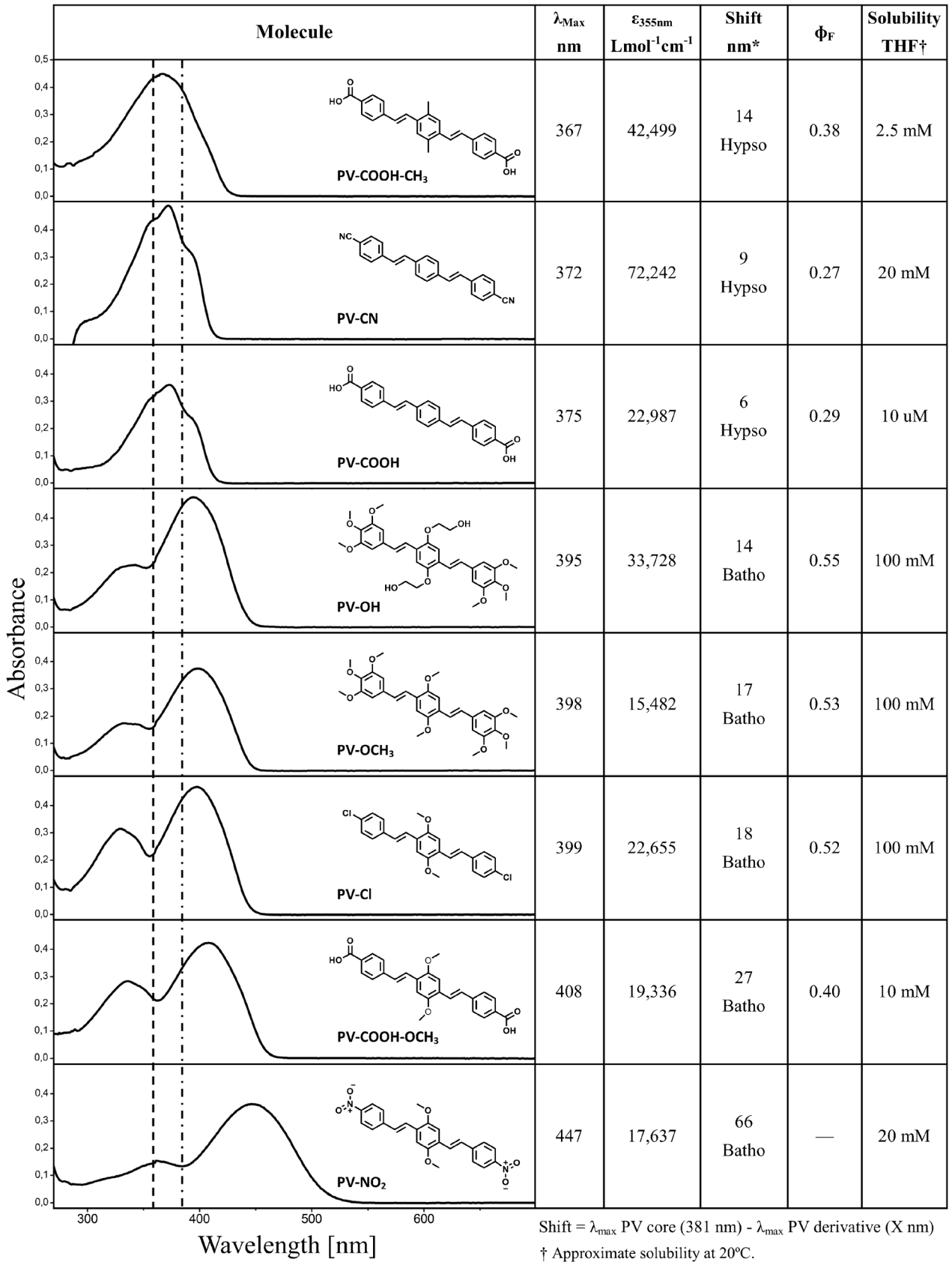

Molecule	λ_{Max} nm	ε_{355nm} $Lmol^{-1}cm^{-1}$	Shift nm*	Φ_F	Solubility THF†
PV-COOH-CH_3	367	42,499	14 Hypso	0.38	2.5 mM
PV-CN	372	72,242	9 Hypso	0.27	20 mM
PV-COOH	375	22,987	6 Hypso	0.29	10 uM
PV-OH	395	33,728	14 Batho	0.55	100 mM
PV-OCH_3	398	15,482	17 Batho	0.53	100 mM
PV-Cl	399	22,655	18 Batho	0.52	100 mM
PV-COOH-OCH_3	408	19,336	27 Batho	0.40	10 mM
PV-NO_2	447	17,637	66 Batho	—	20 mM

Shift = λ_{max} PV core (381 nm) - λ_{max} PV derivative (X nm)

† Approximate solubility at 20ºC.

Figure 1. Photophysical properties for PVs derivatives. Dashed and dashed-dotted lines correspond to the laser wavelength (355 nm) and the PV core maximum absorption wavelength (381 nm), respectively

primary ions under these conditions. Analysis of molar absorptivity values at 355 nm (ε_{355nm}) allow for comparison between the UV-vis spectral properties of the PV series and established MALDI matrices like DCTB and CHCA in liquid phase. Experimental ε_{355nm} values for CHCA (15,490 L mol^{-1} cm^{-1}) and DCTB (30,144 L mol^{-1} cm^{-1}) are in accordance with reported values [25, 49]. All PV derivatives, with the exception of PV-OCH_3, have ε_{355nm} values above CHCA (>15,490 L $mol^{-1}cm^{-1}$); while PV-CN, PV-COOH-CH_3 and PV-OH have higher ε_{355nm} values than DCTB (> 30.144 L mol^{-1} cm^{-1}). These values indicate efficiently absorption of 355 nm photons by the PV derivatives in liquid phase and perhaps a good mass spectrometric behavior as MALDI matrices. However, this observation is not meaningful from a MALDI mechanistic point of view and only gives a general idea of the matrices' absorption behavior trends in liquid phase. We have to keep in mind that according to the coupled photophysical and chemical dynamics (CPCD) model of UV MALDI, primary ionization events (and also much of the secondary reactions) occur in a condensed-like phase and that ion yields in MALDI strongly depend on the solid state absorption properties of the matrix and the laser characteristics [2, 49–51]. Hence, matrix photophysical properties in condensed phase are the ones that play a crucial role in primary ions generation through processes involving excitation, migration and concentration of energy [50].

Fluorescence Quantum Yields in Solution

We found that non-radiative (Φ_{NF}) and radiative fluorescence (Φ_F) quantum yields for the PV series also depend on molecular structure. The core PV structure is reported to be highly fluorescent in solution with Φ_F of 0.9 [43]. Introduction of substituents dramatically reduces Φ_F for the PV derivatives as Figure 1 clearly shows. CN and acid PVs (PV-CN, PV-COOH, PV-COOH-CH_3, PV-COOH-OCH_3) exhibiting Φ_F values of 0.27 0.29, 0.38 and 0.40 (Φ_{NF} 0.80, 0.71, 0.62 and 0.60), respectively, experience the highest reduction in Φ_F of all the tested PVs. Low Φ_F, or high Φ_{NF} in other words, is mainly attributed by many authors to a severe deformation of the PV planar structure [42, 43]. From a mass spectrometric point of view both yields are important depending on the desired reaction channel during the ionization step. Low Φ_F suggests a relaxation pathway predominantly thermal; an important effect during the desorption step in the MALDI process because is related to heating, expansion and increased matrix/analyte ejection from the solid phase which will eventually improve ion release into the gas phase [52, 53]. Interestingly, a reduction on effective π conjugation length and decreased planarity in PV-CN, PV-COOH and PV-COOH-CH_3 explains both the observation of high Φ_{NF} and the hypsochromic shifts in the UV-vis spectrum for these PV derivatives. On the other hand, PV-Cl, PV-OCH_3, PV-OH exhibit Φ_F yields of 0.52, 0.53 and 0.55, almost equivalent to Φ_{NF}. Although there is still a reduction in Φ_F for these structures, apparently the presence of -Cl and -OCH_3 groups do not disrupt compound planarity to a significant extent.

Interestingly observations by Sierra *et al.* [19] and Heller *et al.* [43] indicate the possibility of intramolecular hydrogen bond formation in PV-OH and PV-OCH_3 analogues, involving the oxygen in the –OCH_3 units in the terminal phenylene rings and the ß carbon of the adjacent vinylene group. These H bonds could reduce planarity while not dramatically, which could explain the observed Φ_F values. Also interestingly, an increase on effective π conjugation length and increased planarity in PV-Cl, PV-OCH_3 and PV-OH explains both the observation of moderate Φ_{NF} and the bathochromic shifts in the UV-vis spectrum for these PV derivatives. Finally, PV-NO_2, due to its red-shifted absorption, did not show any fluorescence at the excitation wavelength of 355 nm; for this reason, the Φ_F value for this derivative is not included in Figure 1.

Mass Spectrometric Characterization

Figure 2 shows positive mode LDI mass spectra for the tested PV derivatives, using 2.5 nmol of each compound on target and a laser power of 0.5 μJ per pulse. No clusters were observed in the mass spectra, where the base peak always corresponds to the PV radical cation ($M^{+\cdot}$). The registered mass accuracy for the $M^{+\cdot}$ species was always below 75 ppm. Upon LDI some of the PV molecular radical cations lose a hydroxyl radical ($^{\cdot}OH$) to produce a low abundance cation; as an example PV-COOH (Figure 2b) shows signals at *m/z* 370.122 and 353.123 corresponding to the molecular ion ($M^{+\cdot}$) and the fragment $[M\text{-}OH]^+$, respectively. A similar behavior is observed for both PV-COOH-CH_3 and PV-COOH-OCH_3 derivatives (Figure 2c and d) where the $M^{+\cdot}$ ions, at *m/z* 398.163 and *m/z* 430.148, are accompanied by the $[M\text{-}OH]^+$ ion at *m/z* 381.156 and *m/z* 413.141, respectively. On the other hand, PV-CN, PV-Cl, PV-NO_2, PV-OH and PV-OCH_3 derivatives (Figure 2a, e, f, g, and h) do not fragment and their radical cations are observed at *m/z* 332.156, 410.091, 432.138, 582.236 and 522.255, respectively; the chlorine characteristic isotopic pattern is clearly distinguishable for the PV-Cl. In addition, experimental isotopic patterns for the PVs (see insets in Figure 2) coincide with the calculated isotopic patterns for each derivative [41].

We also performed LDI experiments under acidic conditions for the eight PV derivatives, using various amounts of TFA, to assess the PVs ability of forming protonated molecules or adducts. We did not observe protonated molecules or adducts of the type $[M+H]^+$ or $[M+Na/K]^+$, despite the presence of polar functionalities in the PV structures. Matrix background signals in the PVs mass spectra are negligible; there is no evidence of clusters, or π-π stacking oligomer formation in the gas phase (Figure 2). Traditional ET matrices such as DCTB and 9-nitroanthracene exhibit extensive adduct formation in MALDI MS which interfere with the analysis of low mass analytes. For instance, in positive ion mode DCTB is not only observed as a molecular radical cation, but also as $[M+H]^+$, $[M+Na]^+$, $[2M+H]^+$ and several other charged species, dominating the low mass range of the MS (See Figure S4 of

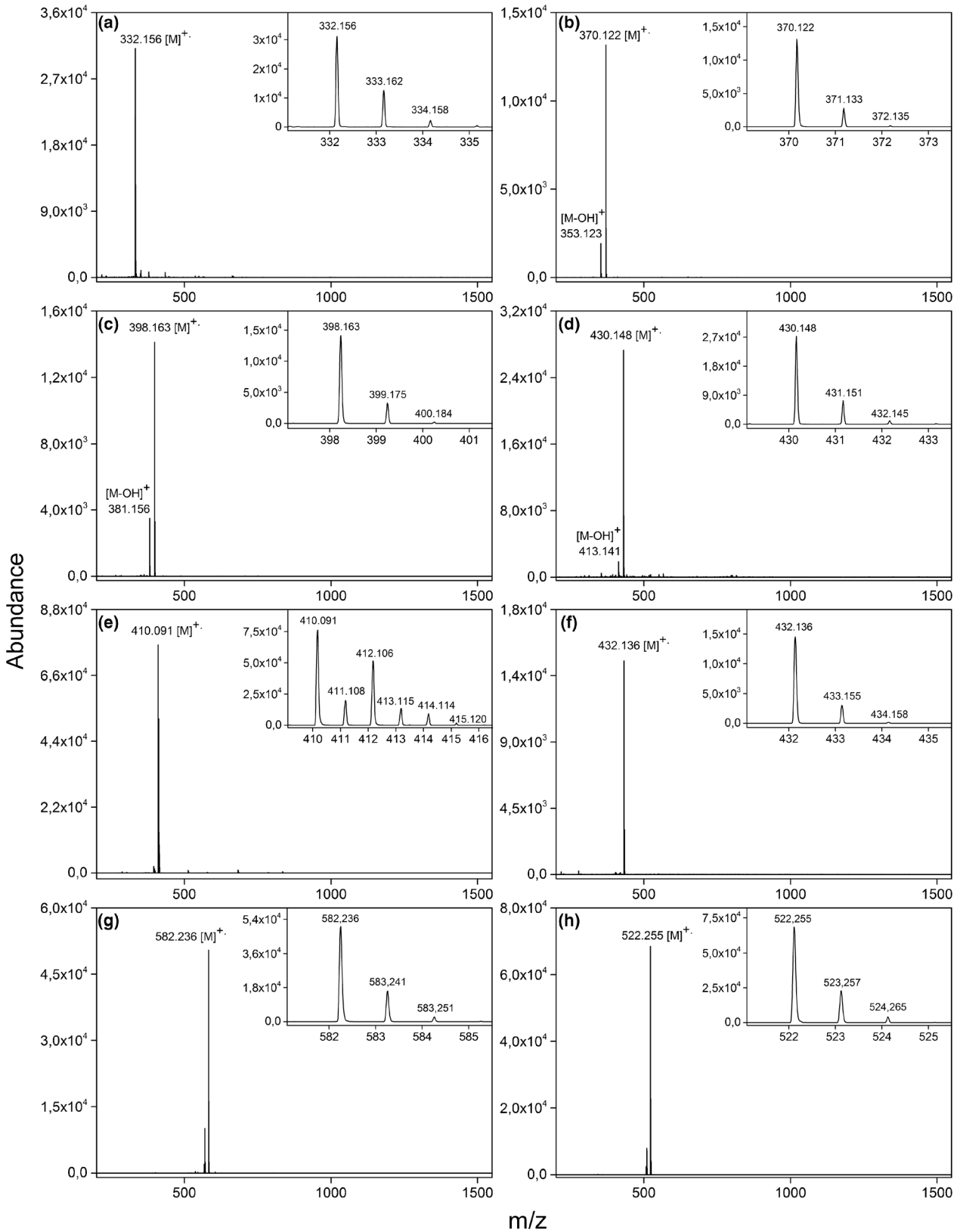

Figure 2. LDI-TOF spectra for the PV derivatives: **(a)** PV-CN, **(b)** PV-COOH, **(c)** PV-COOH-CH_3, **(d)** PV-COOH-OCH_3, **(e)** PV-Cl, **(f)** PV-NO_2, **(g)** PV-OH, **(h)** PV-OCH_3. Inserts show experimental isotopic distributions. See Table S3 of the Supplemental Information or molecular ion ($M^{+\cdot}$) isotopic abundances and mass accuracy data

the Supplemental information) [25]. Likewise, 9-nitroanthracene produces π-π stacking adduct ions detected in the *m/z* 200-800 range [5]. PVs, on the other hand could be potentially useful for characterization of either low or high mass analytes.

Using the same amount of each PV derivative and the standard matrix DCTB (2.5 nmol on target) we increased the laser power from 0.14 to 2.5 μJ per pulse and determined the detection threshold (the lowest laser power needed to get a molecular ion signal with S/N>3) and the ion appearance curves for all tested molecules as seen in Figure 3. Under the same experimental conditions, the power threshold for ion detection for all PV derivatives is always lower than that of the standard DCTB matrix, while molecular ion abundances for the PV derivatives are always higher than for DCTB. Molecular ions for PV-OCH_3, PV-Cl and PV-OH exhibit detection thresholds of 0.14, 0.17 and 0.22 μJ, respectively; while PV-COOH-CH_3, PV-COOH, PV-NO_2, PV-CN and PV-COOH-OCH_3 show higher thresholds of 0.27, 0.27, 0.34, 0.47 and 0.47 μJ, respectively. Under our experimental conditions the DCTB detection threshold was 0.58 μJ. For analytical purposes, a laser power of two or three times over that of the matrix ion threshold is always recommended. In the case of the PV derivatives those values are extremely low when compared with the standard DCTB, this fact translates into analytical applications using PVs as matrices requiring less laser power. This could not only benefit the instrument hardware, in terms of laser durability and internal surfaces cleaning, but also its analytical performance in terms of mass accuracy, sensitivity and resolution.

Above the detection threshold ion abundances increase rapidly with increased laser power and then level out, as observed in the ion appearance curves for the PV series in Figure 3. The linear section of the experimental ion appearance curve can be fitted to a power function of the type $Y \sim H^m$ [54], where Y is the ion abundance, H the laser power and m depends on the matrix performance. For the tested PV derivatives m ranges from 5.5 up to 9.47; while for DCTB m corresponds to 4.45. Clearly, under identical experimental conditions PV derivatives have not only the ability to efficiently absorb energy but also to produce more ions, when compared to the standard DCTB matrix. In Figures S5 and S6 of the Supplemental Information we include an analysis of signal to noise (S/N) ratio and resolution for PV derivatives and DCTB molecular ions as a function of laser pulse energy.

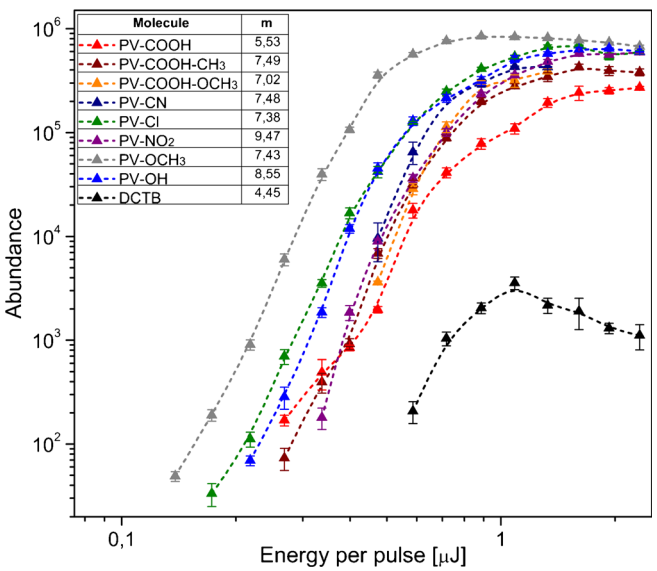

Figure 3. Appearance curves for PV derivatives and DCTB molecular ions ($M^{+\cdot}$)

Ionization Potential (IP) Calculations

Figure 4 shows PV derivatives IPs calculated using the Electron Propagator Theory - EPT. According to Ortiz EPT provides one of the most reliable tools for accurate IP calculation; the author demonstrates this fact comparing experimental IP values, from photoelectron spectroscopy, with theoretical values from EPT [39, 40]. For IP calculations of highly conjugated systems such as PVs, EPT was proven to be a valuable tool. However, a detailed description of the theoretical considerations involved in IP calculations is out of the scope of this paper and will be addressed as a separate contribution. It is well know that the ET processes occurs through a two-step ionization mechanism where the matrix (M) is first photoionized to produce a radical cation according to (Equation 1), and then undergoes an ET reaction with the analyte (A) to produce an analyte radical

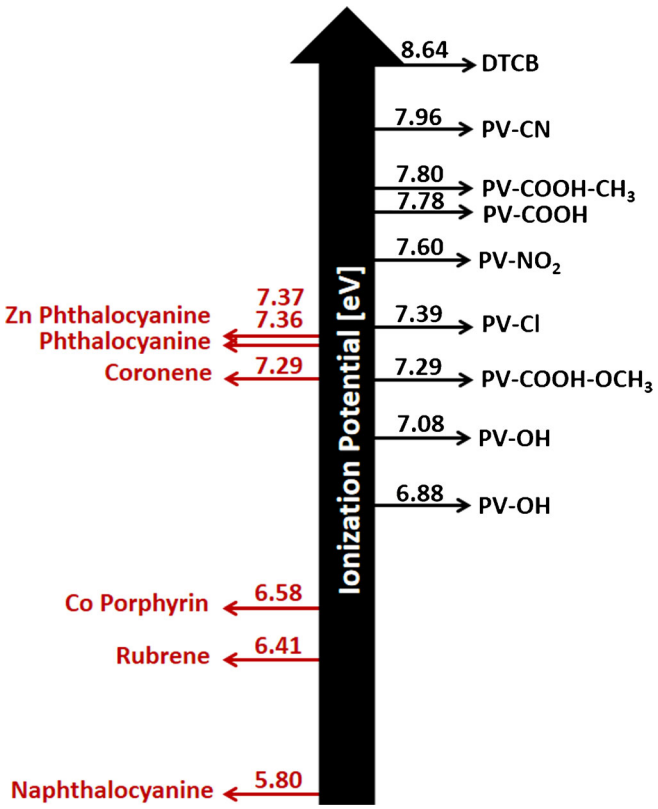

Figure 4. Ionization potentials for PV derivatives calculated using Electron Propagator Theory – EPT (right). Analytes IPs correspond to reported values (left) [13–15]

cation and a matrix neutral molecule in the gas phase (Equation 2) [7, 52].

$$M + nhv \rightarrow M^{+\cdot} \quad (1)$$

$$M^{+\cdot} + A \rightarrow M + A^{+\cdot} \quad (2)$$

Limbach *et al.* [7, 53] suggested that analyte radical cation formation only occurs if the recombination energy of the matrix exceeds the recombination energy of the analyte. Approximating the recombination energy of both matrix and analytes to the vertical ionization potentials, they proposed the well-known criterion $IP_{(M)}>IP_{(A)}$ for the ET processes to happen. Interestingly they also observed that analyte ion abundances are directly related to the IP differences between matrix and analyte, with higher differences indicating a more favorable electron transfer process [52, 53]. Consequently, knowing the IP for ET matrices in MALDI is of fundamental importance for analytical applications. High IP values are desirable for ET MALDI matrices, although not so high that the photoionization process does not occur under MALDI conditions. Commonly IP values for commercially available ET matrices range from 7.0 eV for 9,10-diphenylanthracene [30] to 8.22 eV for DCTB [52]. Our calculations indicate that IPs for the PV derivatives range from 6.88 eV for PV-OCH_3 to 7.96 eV for PV-CN. The highest IP of the series for PV-CN is due possibly to a synergistic effect between the presence of the -CN electron withdrawing group which directly affects the π electronic conjugation system and a considerable planarity disruption in this derivative, as discussed previously. IP values for the tested analytes (see below) are also included in Figure 4 and correspond to reported values [55–57].

Analytical Performance of PV Derivatives as MALDI ET Matrices

In Figures S7 and S8 of the Supplemental Information we show the results of preliminary experiments where we tested the performance of the eight PV derivatives as electron transfer matrices for the ionization of a single analyte NP (naphtho[2,3-a]pyrene; $M^{+\cdot}$ at *m/z* 302.109, IP:6.89 eV) using a laser output of 1.3 μJ per pulse and analyte:matrix ratios of 1:10 (250 pmol), 1:100 (25 pmol), 1:1000 (2.5 pmol), and 1:10,000 (0.25 pmol). At the lowest tested NP concentration (0.25 pmol), the best performance in terms of average S/N ratios was shown by PV-COOH, PV-Cl, PV-COOH-CH_3, and PV-CN with values of 27, 29, 138, and 515 for the NP molecular ion, respectively. Since the S/N ratio for NP with DCTB was 9, we observed S/N net enhancements of 3, 3.2, 15.3, and 57 times for NP when using PV-COOH, PV-Cl, PV-COOH-CH_3, and PV-CN. These S/N enhancements correlate well with IP differences between analyte:matrix as reported previously by Limbach et al. [7, 53]. Three of these four matrices (PV-Cl, PV-COOH-CH_3, and PV-CN) were selected to carry out further experiments with additional analyte molecules; the PV-COOH due to its low solubility was not included and we used instead PV-COOH-OCH_3.

Figure 5 shows the structures of the standard compounds (cobalt porphyrin, phthalocyanine, naphthalocyanine, zinc phthalocyanine, rubrene, coronene) tested as additional analytes, and the S/N ratios of their radical cations using PV-Cl, PV-COOH-CH_3, PV-COOH-OCH_3, PV-CN, and DCTB as matrices with different analyte to matrix molar ratios. All the experiments were performed five times using a laser output of 0.8 μJ per pulse, a suitable working value for the PV derivatives as seen in Figure 3, and the reported data correspond to an average value of these measurements. These analytes readily form radical cations and are commonly studied by LDI using high concentrations. LDI requires harsh conditions such as increased laser power, which commonly induces fragmentation and decreases molecular ion survival yields.

The variation in the S/N value for the cobalt porphyrin (*m/z* 791.206) using PV-CN, PV-COOH-CH_3, PV-COOH-OCH_3, PV-Cl, and DCTB as matrices and different analyte:matrix molar ratios is shown in Figure 5a (see also Figure S9 of the Supplemental Information). When the analyte:matrix ratios vary, from 1:100 to 1:500 and 1:1000, the analyte amount on target decrease from 25 to 5.0 and 2.5 pmol, respectively. No signal for *m/z* 791.206 was observed by either LDI or MALDI when using DCTB and PV-COOH-OCH_3 as matrices. In contrast, MALDI experiments, using PV-CN, PV-Cl, and PV-COOH-CH_3, showed significant S/N values for the radical cation *m/z* 791.206, ranging from 3217 to 348. Among the tested PV derivatives, the PV-CN matrix displays the best performance for the cobalt porphyrin analysis. For instance, an analyte:matrix ratio of 1:100 (25 pmol of cobalt porphyrin) afforded the highest S/N ratio (3217) for *m/z* 791.206 using PV-CN, whereas no signal is observed at the same analyte concentration using LDI. High analyte:matrix ratios, in the order of 1:1 to 1:100, are commonly used on ET ionization experiments [3, 6, 30, 53]. However, when using PV-CN, PV-Cl, and PV-COOH-CH_3 derivatives as MALDI matrices, low analyte:matrix ratios (1:1000, 2.5 pmol on target) provide S/N values of 1006, 614, and 348 for *m/z* 791.206, respectively.

Along the same lines, Figure 5b shows the variation of S/N values for the phthalocyanine (*m/z* 514.165); no signal for this compound was registered using LDI or MALDI with DCTB as matrix (see also Figure S10 of the Supplemental Information). However, phthalocyanine radical cation signals at *m/z* 514.165 were readily observed with high abundances for MALDI experiments with PV-CN, PV-Cl, PV-COOH-CH_3, and PV-COOH-OCH_3 as matrices. In a similar fashion to Figure 5a, the use of PV-CN as matrix improves considerably the S/N of the phthalocyanine molecular ion (*m/z* 514.165). In addition, low analyte:matrix ratios (1:1000, 2.5 pmol on target) can be used and still observe significant S/N ratios of 1579, 894, 197 and 114 for *m/z* 514.165, using PV-CN, PV-Cl, PV-COOH-OCH_3 and PV-COOH-CH_3 respectively. Figure 5c shows the S/N values for the naphthalocyanine radical cation (*m/z* 714.228). This molecule exhibits low ionization efficiency and only the use of relatively high analyte:matrix ratios

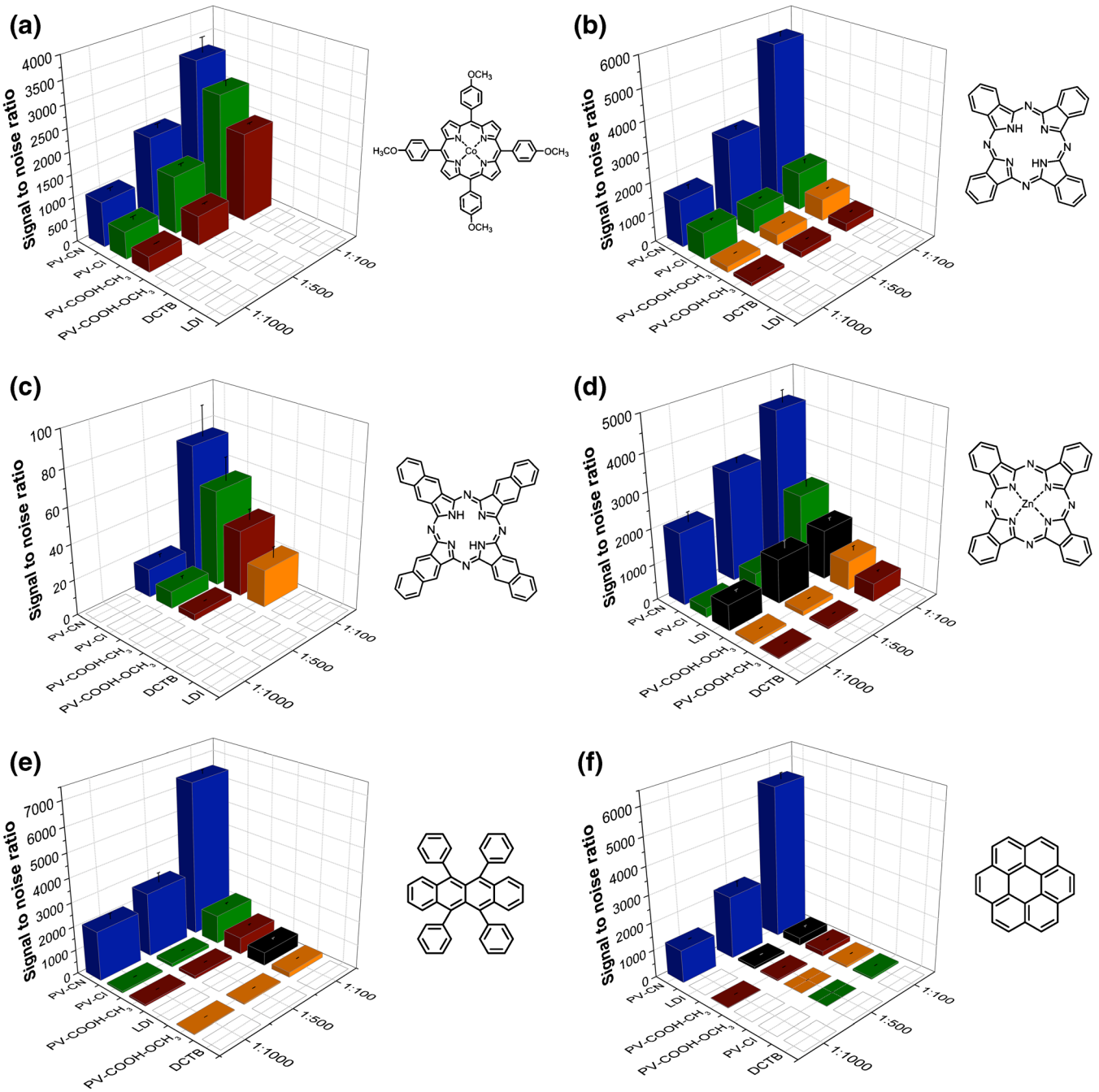

Figure 5. Effect of different matrices and analyte:matrix ratios on S/N values for analyte's radical cations of **(a)** cobalt porphyrin, **(b)** phthalocyanine, **(c)** naphthalocyanine, **(d)** zinc phthalocyanine, **(e)** rubrene, **(f)** coronene

(1:100 and 1:500, corresponding to 25 and 5.0 pmol on target) results on signal observation with S/N values of 75, 54, 37, and 21 using PV-CN, PV-Cl, PV-COOH-CH_3, and PV-COOH-OCH_3 as matrices. No signal was registered for naphthalocyanine, even at high analyte:matrix molar ratios when using LDI or DCTB as matrix.

Figure 5d, e, and f show the variation in S/N of zinc phthalocyanine (*m/z* 576.079), rubrene (*m/z* 532.219), and coronene (*m/z* 300.094) (see Figures S11, S12, and S13 of the Supplemental Information for mass spectra). Interestingly these three analytes exhibit discernible signals under LDI conditions (25 pmol on target), corresponding to S/N ratios of 1397, 557, and 284, respectively. Comparison of the LDI S/N values for these compounds with the values registered when using PV-CN gives us an idea of the role of this PV derivative as ET matrix. Using also the same experimental conditions as in the LDI experiment (25 pmol of analyte on target), the S/N values for the MALDI experiment with PV-CN as matrix are 4246, 6497, and 5569, respectively, for zinc phthalocyanine, rubrene, and coronene, values which correspond to an

Table 1. Detection Limits for Analyte Signals Using PV Derivatives as MALDI ET Matrices

Analyte	LDI	PV-CN	PV-Cl	PV-COOH-CH_3
Co porphyrin	125 pmol	2.5 fmol	2.5 fmol	12.5 fmol
Rubrene	12.5 pmol	2.5 fmol	125 fmol	250 fmol
Coronene	2.5 pmol	12.5 fmol	2.5 pmol	1.25 pmol
Zn pphthalocyanine	125 fmol	2.5 fmol	12.5 fmol	1.25 pmol

enhancement in the molecular ions S/N ratio of 304%, 1166%, and 1961%.

As a general conclusion from Figure 5, we can state that the PV-CN derivative stands out as ET MALDI matrix since it considerably increases molecular ions yield during the ET process, as observed by a dramatic increase in S/N for all tested analytes. We believe that this fact is a combination of the excellent photophysical properties of PV-CN, such as the highest molar absorptivity of all tested PV derivatives (72,242 $Lmol^{-1}cm^{-1}$), low energy threshold (0.47 μJ), and physicochemical characteristics such as high solubility (20 mM), and high ionization potential (7.96 eV). In addition, the PV-CN is the derivative that will undergo the most energetically favorable ET process with the studied analytes because of the energetic condition: $IP_M > IP_A$ (M=matrix, A=analyte).

In Figure S15 of the Supplemental Information, we analyzed the ion appearance curves for four analytes (zinc phthalocyanine, cobalt porphyrin, coronene, and rubrene) and the evolution of S/N ratios as a function of laser pulse energy using different PV matrices. Under the same experimental conditions, we observe that the $M^{+\cdot}$ abundances for all analytes are always higher when using PV-CN as matrix, even at low laser power (0.4 μJ); this observation supports our conclusions from Figure 5. Figure S15 also indicates that the ideal working energies for the PV matrices lie around 0.8 μJ (where the highest S/N ratios for the analytes are recorded), which is almost a 40% decrease in working laser energy from traditional matrices like CHCA, DCTB, and DHB, usually above 1.3 μJ. A matrix that efficiently performs at low laser energy constitutes a major advantage in MALDI because it can not only increase laser lifetime and generate less source contaminations but also hinder fragmentation of labile analytes, increasing ion survival yields as will be illustrated in a future report.

Finally, LODs for four analytes in Figure 5 were calculated using PV-CN, PV-Cl, and PV-COOH-CH_3 derivatives as MALDI matrices because of their high performance. For LODs calculation, analyte concentration was varied from 125 μM to 2.5 nM (125 pmol to 2.5 fmol on target), while maintaining the same matrix concentration (1.25 mM or 1.25 nmol on target); the results are shown in Table 1. For Co-porphyrin analysis, PV derivatives afford LODs six orders of magnitude lower than LDI, and one order of magnitude lower that LDI for Zn-phthalocyanine. Previously, LODs for phthalocyanines using retinoic acid as MALDI matrix were reported at 24 pmol [58], whereas for the PV matrices the LODs are as low as 2.5 fmol (PV-CN) as reported in Table 1. For aromatic compounds analysis, PV derivatives allow detection of rubrene and coronene in concentrations three orders of magnitude below the LODs with LDI. PV-CN, in particular, allowed detection of low-fmol amounts of the four analytes, in contrast with LDI where analytes were observed in the range of pmol to higher fmol.

Conclusions

Unlike proton-transfer reactions in UV-MALDI, involving several ion formation mechanisms, electron-transfer reactions almost exclusively rely on the formation of primary ions through matrix photoionization. From the point of view of the CPCD model [2, 50, 51] excitation and concentration of energy in the matrix network causes "pooling" events that eventually induce matrix ionization. For these pooling events to happen, energy mobility within the matrix molecules is of fundamental importance; these "mobile excitations" are known as molecular excitons. Molecular excitons are capable of energy transfer processes, depending on intermolecular distances between the molecular species, and have lifetimes on the order of nanoseconds.

According to our observations, radical cation formation in PV derivatives occurs at much lower laser powers than current ET matrices such as DCTB. In addition, not only signal abundances for both matrix and analyte are significantly enhanced but also resolution and sensitivity are improved when using PV derivatives in ET processes. We believe that the reason behind these observations lies in the outstanding photophysical properties of PV derivatives. Several literature reports describe exciton formation in high yields, with lifetimes of nanoseconds, when PVs interact with electromagnetic radiation [59, 60]. In addition, PVs forming π stacking structures with interplanar distances of less than 8 Å can have an efficient conjugation between their HOMO and LUMO states, making the exciton formation process in solid phase more favorable [61]. We have previously reported, by X-ray measurements, an interplanar distance for PV-OCH_3 of 4.1 Å [19]. Considering the initial laser/matrix interaction in ET MALDI occurring in condensed phase, we believe that an efficient π–π stacking, combined with long exciton lifetimes, in the tested PV derivatives, could explain the excellent performance of these molecules as electron transfer matrices for UV-MALDI.

In addition, we also demonstrate the use of PV derivatives (PV-CN, PV-COOH-CH_3, PV-COOH-OCH_3, and PV-Cl) as electron-transfer MALDI matrices for the analysis of metal complexes and aromatic compounds. The use of these matrices, particularly PV-CN and PV-Cl, increase the S/N ratio of model analytes two to three orders of magnitude compared

with LDI measurements. Working laser energy for PVs lies in the 0.4–1.0 μJ range, much lower than the laser energy used for traditional matrices like CHCA, DCTB, and DHB, usually above 1.3 μJ. Lower laser energies in MALDI translate into increased laser lifetime and decreased source contamination. In addition, we observed limits of detection in the low fmol range for PV-CN, whereas LDI provides LODs in the pmol to higher fmol range. The observation of low LODs when using the PV matrices supports the idea of ionization through electron transfer from the analyte to the matrix, rather than from direct photoionization. Finally, among the tested PV matrices, PV-CN stands out as ET MALDI matrix because of its high analytical performance.

Acknowledgments

The authors acknowledge funding from COLCIENCIAS (Grant 0041-2013). They also thank Guatiguará Technology Park and the Central Research Laboratory Facility at Universidad Industrial de Santander for infrastructural support. L.J.C. acknowledges the Vice Chancellor for Research Office at Universidad Industrial de Santander (VIE-UIS) for a travel grant.

References

1. Wyatt, M.F.: MALDI-TOFMS analysis of coordination and organometallic complexes: a nic(h)e area to work in. J. Mass Spectrom. **46**, 712–719 (2011)
2. Knochenmuss, R.: Ion formation mechanisms in UV-MALDI. Analyst. **131**, 966–986 (2006)
3. Streletskii, A.V., Ioffe, I.N., Kotsiris, S.G., Barrow, M.P., Drewello, T., Strauss, S.H., Boltalina, O.V.: In-plume thermodynamics of the MALDI generation of fluorofullerene anions. J. Phys. Chem. A. **109**, 714–719 (2005)
4. Suzuki, T., Midonoya, H., Shioi, Y.: Analysis of chlorophylls and their derivatives by matrix-assisted laser desorption/ionization-time-of-flight mass spectrometry. Anal. Biochem. **390**, 57–62 (2009)
5. Brown, T., Clipston, N.L., Simjee, N., Luftmann, H., Hungerbühler, H., Drewello, T.: Matrix-assisted laser desorption/ionization of amphiphilic fullerene derivatives. Int. J. Mass Spectrom. **210/211**, 249–263 (2001)
6. Skelton, R., Dubois, F., Zenobi, R.: A MALDI sample preparation method suitable for insoluble polymers. Anal. Chem. **72**, 1707–1710 (2000)
7. McCarley, T.D., McCarley, R.L., Limbach, P.A.: Electron-transfer ionization in matrix-assisted laser desorption/ionization mass spectrometry. Anal. Chem. **70**, 4376–4379 (1998)
8. Friend, R.H.: Conjugated polymers. New materials for optoelectronic devices. Pure Appl. Chem. **73**, 425–430 (2001)
9. McNeill, C.R., Greenham, N.C.: Conjugated-polymer blends for optoelectronics. Adv. Mater. **21**, 3840–3850 (2009)
10. AlSalhi, M.S., Alam, J., Dass, L.A., Raja, M.: Recent advances in conjugated polymers for light emitting devices. Int. J. Mol. Sci. **12**, 2036–2054 (2011)
11. Chen, S., Jen, T., Lu, H.: A review on the emitting species in conjugated polymers for photo- and electro-luminescence. J. Chinese Chem. Soc. **57**, 439–458 (2010)
12. Luo, F.-T., Tao, Y.-T., Ko, S.-L., Chuen, C.-H., Chen, H.: Efficient electroluminescent material for light-emitting diodes from 1,4-distyrylbenzene derivatives. J. Mater. Chem. **12**, 47–52 (2002)
13. Cornil, J., dos Santos, D., Beljonne, D., Brédas, J.: Electronic structure of phenylene vinylene oligomers: influence of donor/acceptor substitutions. J. Phys. Chem. **99**, 5604–5611 (1995)
14. Díaz, C., Alzate, D., Rodríguez, R., Ochoa, C., Sierra, C.A.: High yield and stereospecific synthesis of segmented poly (p-phenylenevinylene) by the Heck Reaction.pdf. Synth. Met. **172**, 32–36 (2013)
15. Alzate, D., Hinestroza, J.P., Sierra, C.A.: High-yield synthesis of the novel E,E-2,5-dimethoxy-1,4-bis[2-(4-ethylcarboxylatestyril)]benzene by the Heck Reaction. Synth. Commun. **43**, 2280–2285 (2013)
16. Amrutha, S.R., Jayakannan, M.: Probing the pi-stacking induced molecular aggregation in pi-conjugated polymers, oligomers, and their blends of p-phenylenevinylenes. J. Phys. Chem. B. **112**, 1119–1129 (2008)
17. Schenning, A.P.H.J., van Herrikhuyzen, J., Jonkheijm, P., Chen, Z., Würthner, F., Meijer, E.W.: Photoinduced electron transfer in hydrogen-bonded oligo(p-phenylene vinylene)-perylene bisimide chiral assemblies. J. Am. Chem. Soc. **124**, 10252–10253 (2002)
18. Sierra, C., Lahti, P.: A simple multichromophore design for energy transfer in distyrylbenzenes with pyrene pendants. J. Phys. Chem. A. **110**, 12081–12088 (2006)
19. Sierra, C.A., Lahti, P.M.: A photoluminescent, segmented oligo-polyphenylenevinylene copolymer with hydrogen-bonding pendant chains. Chem. Mater. **16**, 55–61 (2004)
20. Praveen, V.K., Ranjith, C., Bandini, E., Ajayaghosh, A., Armaroli, N.: Oligo(phenylenevinylene) hybrids and self-assemblies: versatile materials for excitation energy transfer. Chem. Soc. Rev. **43**, 4222–4242 (2014)
21. Samori, S., Hara, M., Tojo, S., Fujitsuka, M., Majima, T.: Important factors for the formation of radical cation of stilbene and substituted stilbenes during resonant two-photon ionization with a 266- or 355-nm laser. J. Photochem. Photobiol. A – Chem. **179**, 115–124 (2006)
22. Grozema, F.C., Candeias, L.P., Swart, M., van Duijnen, P.T., Wildeman, J., Hadziioanou, G., Siebbeles, L.D.A., Warman, J.M.: Theoretical and experimental studies of the opto-electronic properties of positively charged oligo(phenylene vinylene)s: effects of chain length and alkoxy substitution. J. Chem. Phys. **117**, 11366–11378 (2002)
23. Srinivasan, N., Haney, C.A., Lindsey, J.S., Zhang, W., Chait, B.T.: Investigation of MALDI-TOF mass spectrometry of diverse synthetic metalloporphyrins, phthalocyanines, and multiporphyrin arrays. J. Porphyrins Phthalocyanines. **3**, 283–291 (1999)
24. Streletskiy, A.V., Goldt, I.V., Kuvychko, I.V., Ioffe, I.N., Sidorov, L.N., Drewello, T., Strauss, S.H., Boltalina, O.V.: Application of 9-nitroanthracene as a matrix for laser desorption/ionization analysis of fluorinated fullerenes. Rapid Commun. Mass Spectrom. **18**, 360–362 (2004)
25. Ulmer, L., Mattay, J., Torres-garcia, H.G., Luftmann, H.: Letter: the use of 2- [(2E) -3- (4-tert-butylphenyl) -2- methylprop-2-enylidene] malononitrile as a matrix for matrix-assisted laser desorption/ionization mass spectrometry. Eur. J. Mass Spectrom. **52**, 49–52 (2000)
26. Winter, J., De Gaelle, D., Boon, F., Coulembier, O., Dubois, P., Gerbaux, P.: MALDI-TOF analysis of polythiophene: use of trans-2-[3-(4-t-butylphenyl)-2-methyl-2-propenylidene]malononitrile – DCTB – as matrix. J. Mass Spectrom. **46**, 237–246 (2011)
27. Kumar, M.R., Raju, N.P., Reddy, T.J., Narahari, A., Reddy, M.J.R., Vairamani, M.: Evaluation of methyl 3-(4-methoxy-1-naphthyl)-(E)-2-propenoate and methyl 5-(4-methoxy-1-naphthyl)-(2E,4E)-2,4-pentadienoate as new charge-transfer matrices for matrix-assisted laser desorption/ionization mass spectrometry. Rapid Commun. mass Spectrom. **19**, 3171–3174 (2005)
28. Wyatt, M.F., Stein, B.K., Brenton, A.G.: Characterization of various analytes using matrix-assisted laser desorption / ionization time-of-flight mass spectrometry and 2-[(2E)-3-(4-tert-butylphenyl)-2-methylprop-2-enylidene] malononitrile matrix. Anal. Chem. **78**, 199–206 (2006)
29. Lou, X., de Waal, B.F.M., van Dongen, J.L.J., Vekemans, J.A.J.M., Meijer, E.W.: A pitfall of using 2-[(2E)-3-(4-tert-butylphenyl)-2-methylprop-2-enylidene]malononitrile as a matrix in MALDI TOF MS: chemical adduction of matrix to analyte amino groups. J. Mass Spectrom. **45**, 1195–1202 (2010)
30. Boutaghou, M.N., Cole, R.B.: 9,10-Diphenylanthracene as a matrix for MALDI-MS electron transfer secondary reactions. J. Mass Spectrom. **47**, 995–1003 (2012)
31. Kim, S.O., Jung, H.C., Lee, M.-J., Jun, C., Kim, Y.-H., Kwon, S.-K.: Synthesis and characterization of 9,10-diphenylanthracene-based blue light emitting materials. J. Polym. Sci., Part A Polym. Chem. **47**, 5908–5916 (2009)
32. Coon, J.J., Syka, J.E.P., Schwartz, J.C., Shabanowitz, J., Hunt, D.F.: Anion dependence in the partitioning between proton and electron transfer in ion/ion reactions. Int. J. Mass Spectrom. **236**, 33–42 (2004)

33. Vasil'ev, Y.V., Khvostenko, O.G., Streletskii, A.V., Boltalina, O.V., Kotsiris, S.G., Drewello, T.: Electron transfer reactivity in matrix-assisted laser desorption/ionization (MALDI): ionization energy, electron affinity and performance of the DCTB matrix within the thermochemical framework. J. Phys. Chem. A. **110**, 5967–5972 (2006)
34. Trimpin, S.: Special Feature : A perspective on MALDI alternatives – total solvent-free analysis and electron transfer dissociation of highly charged ions by laserspray ionization. J. Mass Spectrom. **45**, 471–485 (2010)
35. Cárdenas, J.C., Fadini, L., Sierra, C.A.: Triphenylphosphite and ionic liquids: positive effects in the Heck cross-coupling reaction. Tetrahedron Lett. **51**, 6867–6870 (2010)
36. Allen, M.W.: Measurement of fluorescence quantum yields (Technical note: 52019). Thermo Fisher Scientific, Madison (2010)
37. Melhuish, W.: Quantum efficiencies of fluorescence of organic substances: effect of solvent and concentration of the fluorescent solute. J. Phys. Chem. **65**, 229–235 (1961)
38. Frisch, M.J., Trucks, G.W., Schlegel, H.B., Scuseria, G.E., Robb, M.A., Cheeseman, J.R., Scalmani, G., Barone, V., Mennucci, B., Petersson, G.A., Nakatsuji, H., Caricato, M., Li, X., Hratchian, H.P., Izmaylov, A.F., Bloino, J., Zheng, G., Sonnenberg, J.L., Hada, M., Ehara, M., Toyota, K., Fukuda, R., Hasegawa, J., Ishida, M., Nakajima, T., Honda, Y., Kitao, O., Nakai, H., Vreven, T., Montgomery, J.A.J., Peralta, J.E., Ogliaro, F., Bearpark, M., Heyd, J.J., Brothers, E., Kudin, K.N., Staroverov, V.N., Kobayashi, R., Normand, J., Raghavachari, K., Rendell, A., Burant, J.C., Iyengar, S.S., Tomasi, J., Cossi, M., Rega, N., Millam, M.J., Klene, M., Knox, J.E., Cross, J.B., Bakken, V., Adamo, C., Jaramillo, J., Gomperts, R., Stratmann, R.E., Yazyev, O., Austin, A.J., Cammi, R., Pomelli, C., Ochterski, J.W., Martin, R.L., Morokuma, K., Zakrzewski, V.G., Voth, G.A., Salvador, P., Dannenberg, J.J., Dapprich, S., Daniels, A.D., Farkas, Ö., Foresman, J.B., Ortiz, J. V, Cioslowski, J., Fox, D.J.: Gaussian 09, http://www.gaussian.com/g_tech/g_ur/m_citation.htm (2009)
39. Ortiz, J.V.: Electron propagator theory: an approach to prediction and interpretation in quantum chemistry. Wiley Interdiscip. Rev. Comput. Mol. Sci. **3**, 123–142 (2013)
40. Zakrzewski, V.G., Dolgounitcheva, O., Ortiz, J.V.: Ionization energies of anthracene, phenanthrene, and naphthacene. J. Chem. Phys. **105**, 8748–8753 (1996)
41. Patiny, L., Borel, A.: ChemCalc: a building block for tomorrow's chemical infrastructure. J. Chem. Inf. Model. **53**, 1223–1228 (2013)
42. Farinola, G.M., Cardone, A., Babudri, F., Martinelli, C., Naso, F., Bruno, G., Losurdo, M.: Fluorinated poly(p-phenylenevinylene)s: synthesis and optical properties of an intriguing class of luminescent polymers. Materials (Basel). **3**, 3077–3091 (2010)
43. Heller, A.: Organic liquid scintillators. VI. Substituted distyrylbenzenes: scintillation properties and spectra of absorption and fluorescence. J. Chem. Phys. **40,** 2839–2842 (1964)
44. Kraft, A., Grimsdale, A., Holmes, A.: Electroluminescent conjugated polymers seeing polymers in a new light. Angew. Chem. Int. Ed. Engl. **37**, 402–428 (1998)
45. Moratti, S.C., Cervini, R., Holmes, A.B., Baigent, D.R., Friend, R.H., Greenham, N.C., Gruner, J., Hamer, P.J.: High electron affinity polymers for LEDs. Synth. Met. **71**, 2117–2120 (1995)
46. Saiyed, A.S., Patel, K.N., Kamath, B.V., Bedekar, A.V.: Synthesis of stilbene analogues by one-pot oxidation-Wittig and oxidation-Wittig–Heck reaction. Tetrahedron Lett. **53**, 4692–4696 (2012)
47. Vadehra, G.S., Wall, B.D., Diegelmann, S.R., Tovar, J.D.: On-resin dimerization incorporates a diverse array of pi-conjugated functionality within aqueous self-assembling peptide backbones. Chem. Commun. **46**, 3947–3949 (2010)
48. Sierra, A.F., Rodríguez, R., Sierra, C.A.: Sintesis estereoselectiva de un nitroderivado de fenilvinilideno mediante la reaccion de heck usando fosfitos. Rev. Colomb. Química. **39**, 163–171 (2010)
49. Soltwisch, J., Jaskolla, T.W., Hillenkamp, F., Karas, M., Dreisewerd, K.: Ion yields in UV-MALDI mass spectrometry as a function of excitation laser wavelength and optical and physico-chemical properties of classical and halogen-substituted MALDI matrixes. Anal. Chem. **84**, 6567–6576 (2012)
50. Knochenmuss, R.: A quantitative model of ultraviolet matrix-assisted laser desorption/ionization. J. Mass Spectrom. **37**, 867–877 (2002)
51. Knochenmuss, R.: MALDI mechanisms: wavelength and matrix dependence of the coupled photophysical and chemical dynamics model. Analyst. **139**, 147–156 (2014)
52. Hoteling, A., Nichols, W., Giesen, D., Lenhard, J., Knochenmuss, R.: Electron transfer reactions in laser desorption/ionization and matrix-assisted laser desorption/ionization: factors influencing matrix and analyte ion intensities. Eur. J. Mass Spectrom. **12**, 345–358 (2006)
53. Macha, S.F., McCarley, T.D., Limbach, P.A.: Influence of ionization energy on charge-transfer ionization in matrix-assisted laser desorption/ionization mass spectrometry. Anal. Chim. Acta. **397**, 235–245 (1999)
54. Dreisewerd, K.: The desorption process in MALDI. Chem Rev. **103**, 395–426 (2003)
55. Linstrom, P.J., Mallard, W.G.E.: NIST Chemistry WebBook, NIST Standard Reference Database Number 69. National Institute of Standards and Technology, Gaithersburg, MD
56. Liao, M., Scheiner, S.: Electronic structure and bonding in metal porphyrins, metal = Fe, Co, Ni, Cu. Zn. Chem. Phys. **117**, 205–219 (2002)
57. Ghosh, A., Gassman, P.G., Almlof, J.: Substituent effects in porphyrazines and phthalocyanines. J. Am. Chem. Soc. **116**, 1932–1940 (1994)
58. Chen, Y.-T., Wang, F.-S., Li, Z., Li, L., Ling, Y.-C.: Development of a matrix-assisted laser desorption ionization mass spectrometric method for rapid process-monitoring of phthalocyanine compounds. Anal. Chim. Acta. **736**, 69–77 (2012)
59. Frolov, S.V., Liess, M., Lane, P.A., Gellermann, W., Vardeny, Z.V.: Exciton dynamics in soluble poly (p -phenylene-vinylene): towards an ultrafast excitonic switch. Phys. Rev. Lett. **78**, 4285–4288 (1997)
60. Vijayakumar, C., Praveen, V.K., Kartha, K.K., Ajayaghosh, A.: Excitation energy migration in oligo(p-phenylenevinylene) based organogels: structure-property relationship and FRET efficiency. Phys. Chem., Chem. Phys. **13**, 4942–4949 (2011)
61. Cornil, J., Heeger, A., Brédas, J.: Effects of intermolecular interactions on the lowest excited state in luminescent conjugated polymers and oligomers. Chem. Phys. Lett. **2614**, 463–470 (1997)